Inadequacy of Continuum Solvation for Polar Reactions: Predicting the Mechanism of Carbonyl–Olefin Metathesis

Authors: Hannah L. Vonesh[1], Corin C. Wagen[2], Spencer E. McMinn[3], Joshua B. Thedford[1], Eugene E. Kwan[4,*], Corinna S. Schindler[1,*]

Affiliations:

[1]Department of Chemistry, University of Michigan; 930 North University Ave., Ann Arbor, MI 48109, United States.

[2]Department of Chemistry and Chemical Biology, Harvard University; 12 Oxford St., Cambridge, MA 02138, United States.

[3]Discovery Chemistry, Merck & Co., Inc.; 33 Avenue Louis Pasteur, Boston, MA 02115, United States.

[4]Process Research and Development, Merck & Co., Inc.; 33 Avenue Louis Pasteur, Boston, MA 02115, United States.

*Corresponding author. Emails: eugene.kwan@merck.com, corinnas@umich.edu

Abstract: In carbonyl–olefin metathesis, two π-bonds undergo a cycloaddition-cycloreversion process to form valuable alkenes from simple precursors (*1–18*). Although this synthetic methodology has advanced significantly, further improvements would be greatly facilitated by a clear understanding of whether Lewis-acid-catalyzed carbonyl–olefin metathesis reactions occur via a stepwise or concerted pathway. Here we use $^{12}C/^{13}C$ kinetic isotope effects (KIEs), $^{1}H/^{2}H$ KIEs, and Hammett studies to show that prototypical iron(III)-catalyzed ring-closing carbonyl–olefin metathesis reactions of aryl ketones are stepwise. Despite this strong experimental evidence, typical computational models incorrectly predict a concerted mechanism. We trace this failure to the use of conventional implicit solvation models and demonstrate that when solvent molecules are explicitly represented (*19*, *20*), the correct stepwise mechanism is predicted. These results call into question prior computational proposals of concerted carbonyl-olefin metathesis, highlight the importance of explicit solvent representations for charged intermediates, and have broad implications for how all polar reactions are studied.

One-Sentence Summary: Disagreement between theoretical and experimental kinetic isotope effects reveals a stepwise mechanism for carbonyl–olefin metathesis and points to a common flaw in computational models of polar reactions.

Main Text:

Significant advances in computational methodology have revolutionized the study of organic reaction mechanisms (*21*). Notably, improvements in the performance of density functional theory (DFT) methods now enable mechanistic proposals to be made before experimental studies can be conducted (*22*). The validity of this prospective approach has been supported subsequently by many experimental studies, with particularly compelling evidence emerging from $^{12}C/^{13}C$ KIE studies in which the predicted and observed effects agree closely (*23*–*25*).

The strategy of basing mechanistic proposals on DFT calculations and using KIE measurements for confirmation is especially attractive in the area of Lewis-acid-catalyzed carbonyl–olefin metathesis reactions. This class of transformations has recently received increased attention due to its analogy to olefin–olefin metathesis and the potential of forming valuable alkene products from simple substrates. Accordingly, determining whether carbonyl–olefin metathesis reactions proceed through stepwise or concerted mechanisms (Fig. 1) has become an important goal for groups aiming to leverage mechanistic insight to design improved catalyst systems. However, carbonyl–olefin metathesis reactions have proven to be difficult to study experimentally, and DFT calculations remain our primary guide as to whether a stepwise or concerted mechanism is occurring.

For most Lewis-acid-catalyzed carbonyl-olefin metathesis reactions, DFT predicts stepwise mechanisms; for example, stepwise mechanisms have been predicted for tropylium- (*10*), iodine- (*11*), pTSA-$HFIP_3$- (*15*) and gallium-catalyzed (*13*) reactions. In other systems involving aluminum- (*1*), zinc- (*2*), boron- (*3*), or trityl- (*5*) based carbonyl–olefin metathesis, DFT predictions are not available, but stepwise mechanisms have been proposed by analogy to known polar mechanisms. By contrast, concerted mechanisms have been predicted for a range of iron(III)-catalyzed carbonyl–olefin metathesis reactions (*8*, *18*), while mixed mechanisms involving both stepwise and concerted steps have been proposed in other systems (*7*, *14*).

Given these potentially conflicting proposals, a tremendous effort has been made to gather supporting experimental evidence. While natural abundance $^{12}C/^{13}C$ KIE studies would directly test any proposed mechanism, the required measurements remain technically demanding and impractical due to the requirement for large scale reactions. As a result, a more common strategy for evaluating these mechanistic proposals is to perform trapping experiments (*6–9*, *14*). If a stepwise mechanism is operative, then betaines **7** and **9** form as intermediates, and these carbocationic intermediates could potentially be trapped by nucleophiles.

In some cases, trapping has indeed been observed; in others, carbonyl–olefin metathesis has proceeded normally. However, the mechanistic implications of these observations are unclear. While trapping could be consistent with betaine capture, Lewis acids are known to catalyze oxetane-opening reactions (*26*, *27*). As such, trapping could also be consistent with opening of the oxetane intermediate that is present in both the stepwise and concerted pathways. Similarly, while the absence of trapping might reflect the absence of a betaine intermediate, a negative result could also be explained by a short-lived betaine or an inefficient trapping agent.

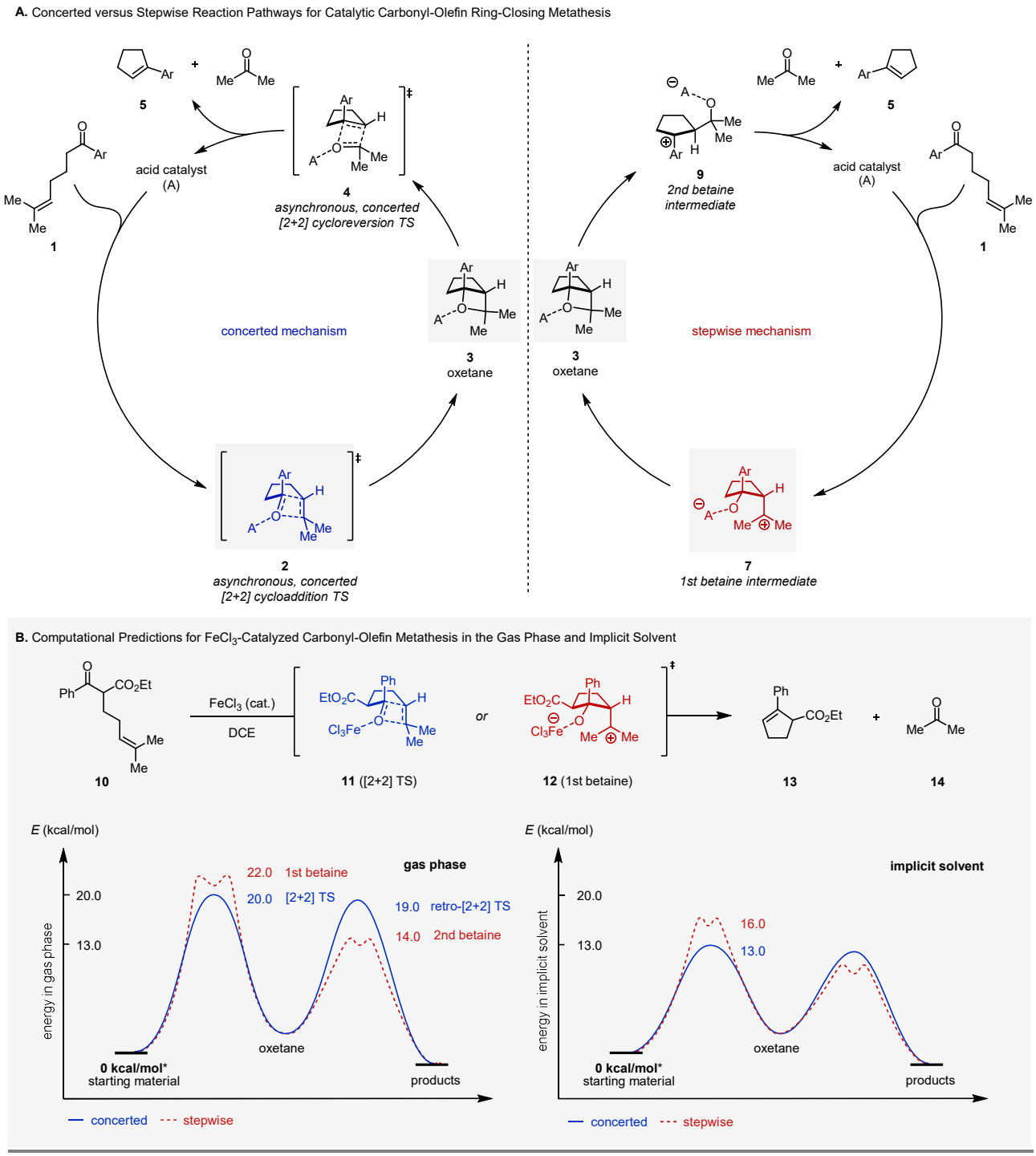

Figure 1. Mechanistic scenarios for carbonyl–olefin metathesis. (a) Asynchronous, concerted and stepwise reaction pathways for Lewis acid-catalyzed carbonyl–olefin metathesis. b) Conventional DFT calculations (B3LYP-D3(BJ)/jul-cc-pVDZ) predict concerted carbonyl–olefin metathesis in both the gas phase and implicit solvent. *Electronic energies are referenced to the pre-complex. Implicit solvent refers to the polarizable continuum model (PCM) (*28*) with DCE. Cycloreversion energies were not calculated in implicit solvent.

In contrast, KIEs offer a more definitive framework for determining whether a given carbonyl–olefin metathesis reaction is stepwise or concerted. A detailed KIE study of a prototypical carbonyl–olefin metathesis reaction might also yield mechanistic insights that inform the design of future reactions. Furthermore, comparing the computational predictions to a full suite of experimental results would directly test the ability of current theoretical methods to model charge-separated intermediates and polar reactions in general.

A prototypical system that is convenient for such a mechanistic study is the iron(III)-trichloride-catalyzed ring-closing metathesis of aryl ketones and prenyl olefins to form cyclopentenes. Before conducting any experiments, we assessed the ability of DFT to make accurate mechanistic predictions by following conventional best practices (*29-31*) by selecting an affordable computational method that closely reproduces the results of high-level calculations. Specifically, we evaluated candidate model chemistries by comparing DFT and coupled cluster (DLPNO-CCSD(T_1)/aug-cc-pVTZ/TightPNO) energies in the gas phase (*32*). To span the stepwise–concerted continuum, we generated structures from a grid of C1–C2 and C3–O1 bond distances (Fig. 1b) such that the test set contained both charge-separated betaines and potentially concerted transition states (Supplementary Section 8).

For most model chemistries, we observed a close correspondence between the DFT and coupled cluster energies, with T_1 diagnostic values for the latter indicating the appropriateness of a single-reference wavefunction for these high-spin iron(III) species (*33*, *34*). Overall, we selected the routine method B3LYP-D3(BJ)/jul-cc-pVDZ as an appropriate model chemistry in terms of dynamic correlation, basis set completeness, and static correlation. We then predicted the mechanism for the carbonyl–olefin metathesis reaction of prenyl substrate **10**. Importantly, in both the gas phase and implicit 1,2-dichloroethane (DCE), the concerted pathway is favored by 2–3 kcal/mol over the stepwise pathway, with cycloaddition (**11**) being rate-determining (Fig. 1).

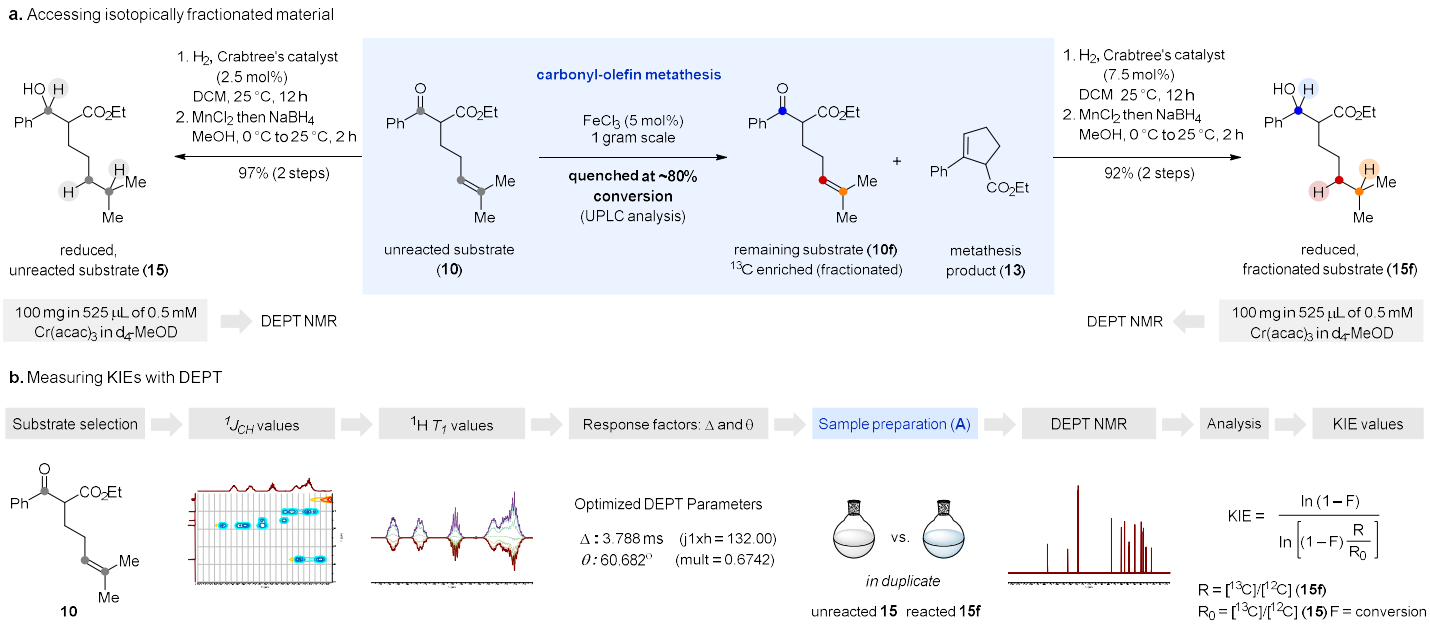

Figure 2. Workflow for $^{12}C/^{13}C$ KIE measurements. (a) KIEs were measured at natural abundance by assessing the isotopic fractionation of recovered vs. unreacted starting materials. Attached protons at the carbons of interest (colored circles) were introduced by a high-yielding two-step reduction sequence that did not affect the isotope ratios. (b) Isotope ratios were measured by DEPT NMR. To ensure that signal:noise was maximized for each carbon of interest, optimal values of the polarization transfer delay (Δ) and read angle (θ) were chosen based on measured $^{1}J_{CH}$ values. Spectroscopic data were collected over 6 days (15 blocks/sample for 4 samples) using a randomized block design. For additional details on data acquisition and analysis, please see Supplementary Section 5.

This computed pathway for concerted carbonyl–olefin metathesis leads to concrete predictions of primary carbon KIEs at C1, C2, and C3 that can be tested experimentally. To accomplish this, we ran an intermolecular competition experiment on substrate **10** at natural abundance and compared the isotope ratios of the unreacted and remaining starting material at ~80% conversion (Fig. 2a). Because the traditional quantitative single-pulse NMR method (*35*) of determining site-specific isotopic fractionations is limited by the poor sensitivity of ^{13}C as an NMR nucleus, we employed our distortionless enhancement by polarization transfer (DEPT) NMR methodology for accelerating natural abundance KIE measurements (Fig. 2b) (*36*). Since this method requires attached protons for sensitivity enhancement, the carbonyl and olefin moieties in **10** were reduced in a two-step sequence with a sufficiently high yield to avoid perturbing the isotopic ratios at C1 and C3 (Fig. 3).

Despite the careful choice of computational method, the predicted KIEs for the concerted cycloaddition and the experimental KIEs disagreed substantially (**11** vs **10**, Fig. 4a). In particular, the discrepancies in the KIEs at the olefinic carbons (0.008 at C2 and 0.014 at C3) were too large to be explained by the choice of model chemistry (Supplementary Section 8e) (*36*). Therefore, the experimental KIEs rule out the concerted mechanism. Interestingly, the predicted equilibrium isotope effects (EIEs) for prenyl betaine **12** matched the experimental values.

Because geometry **12** is a very shallow stationary point and collapses on slight conformational perturbations, it may not be a realistic representation of a true betaine. Therefore, we also considered non-stationary structures with constrained C1–C2 and C3–O1 distances (*37*–*39*). We found that betaine **16** matched the observed KIEs even more closely. These results reinforce the interpretation of a stepwise pathway in which betaine formation is rate-limiting.

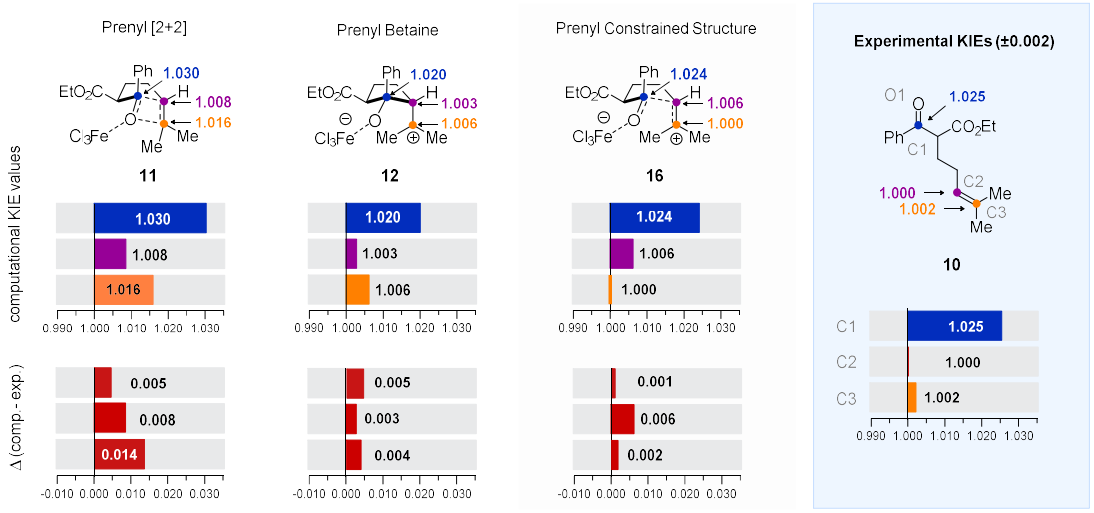

Figure 3. Experimental $^{12}C/^{13}C$ KIEs for prenylated alkenes support a stepwise mechanism. Comparison of computational and experimental carbon KIEs. The KIEs do not match a concerted [2+2] transition state but are similar to the predicted EIEs for the first betaine. A closer match (**16**) to the experimental KIEs was found by considering structures with constrained C1–C2 and C3–O1 bond distances.

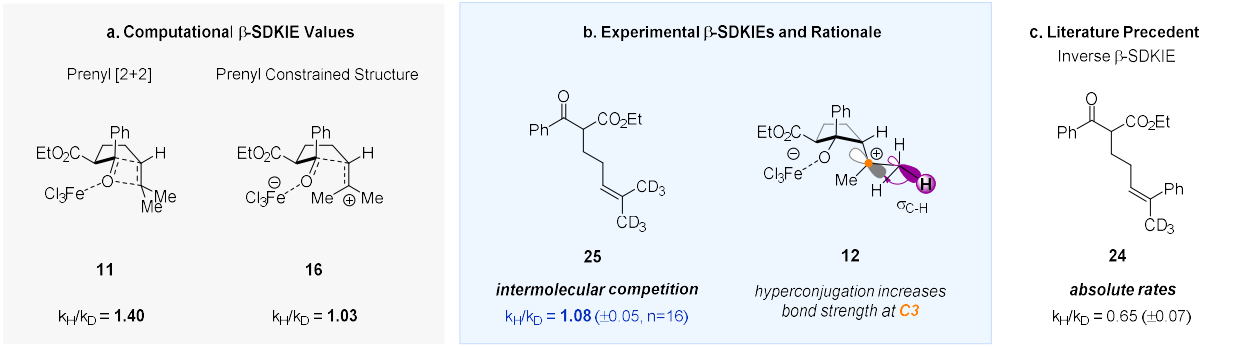

Figure 4. Secondary $^{1}H/^{2}H$ KIE studies. (a) Predicted β-secondary deuterium KIE (β-SDKIE) values for a concerted [2+2] transition state and constrained betaine **16**. (b) Experimental results obtained via intermolecular competition reactions show a normal β-SDKIE. This value is inconsistent with a concerted cycloaddition but matches betaine formation. The KIE at C3 is nearly unity because transition state hyperconjugation increases the local bond strength, countering the loss of the C2=C3 π bond (*40*). (c) An unusual inverse β-SDKIE was previously reported for a related alkene, **24**. This differing result can be rationalized due to the larger errors incurred by absolute rate relative to intermolecular competition experiments.

If betaine formation is rate-limiting, then one would expect to find a normal β-secondary deuterium KIE (SDKIE) due to hyperconjugation (*41,42*) between the methyl groups and the incipient carbocation at C3. When we carried out an intermolecular competition experiment between prenyl substrate **10** and its deuterated isotopologue **25**, we observed a KIE of 1.08±0.05 (Fig. 6b). This value agrees well with the prediction of 1.03 for structure **16**, but not at all with

[2+2] structure **11**, and thus provides further evidence for a stepwise mechanism (*43*). One potential discrepancy comes from the previously reported (*8*) β-secondary deuterium KIE (SDKIE) of 0.65 for styrene **24** (Fig. 4). However, this measurement was obtained by absolute rate measurements, which are subject to greater experimental error than competition experiments.

Rate-limiting betaine formation also implies that a Hammett study would detect positive charge buildup. Because a Hammett study would require switching from prenyl to styrenyl substitution, potentially altering the mechanism, we first measured the KIEs for styrene **20** (Fig. 5). The observed KIEs were qualitatively similar to those for prenyl substrate **10**, with a significant KIE at C1 and small effects at C2 and C3. Once again, these values are inconsistent with a concerted mechanism (**17**) and consistent with a stepwise mechanism (**18** and **19**). This finding that iron(III) induces betaine formation is similar to the behavior of aluminum(III) in carbonyl-ene reactions (*44*), which generates carbocations via a stepwise pathway. Overall, these experiments establish a general mechanistic framework for the study of carbonyl–olefin metathesis reactions, and should inform future reaction and catalyst design.

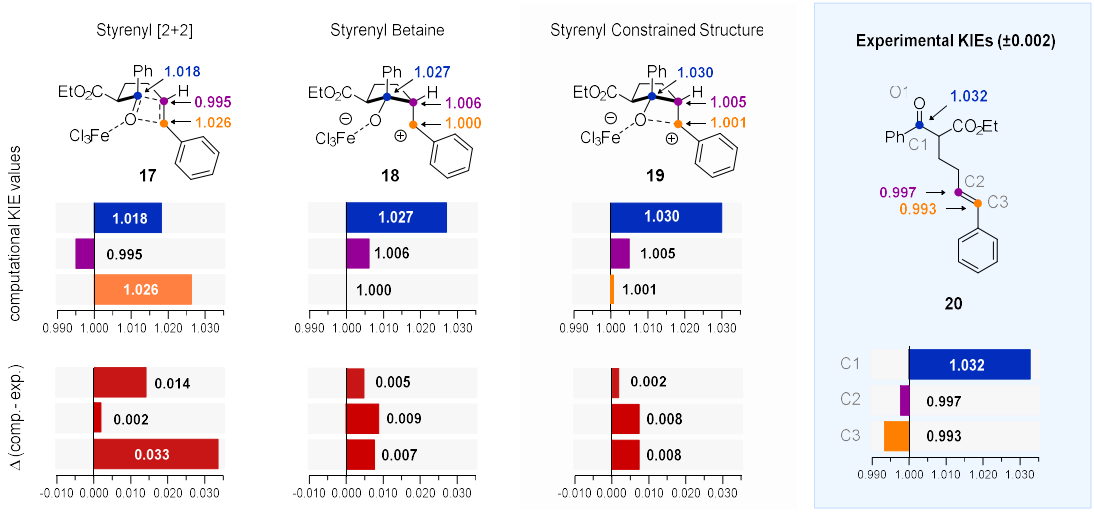

Figure 5. Experimental $^{12}C/^{13}C$ KIEs for styrenyl alkenes support a stepwise mechanism. The experimental KIEs for styrenyl substrate **17** are also consistent with a stepwise mechanism. The observed values are similar to those for prenyl substrate **10**, indicating that both substrate classes proceed via the same mechanism and the findings of the Hammett study (Figure 6) will generalize to other substrates.

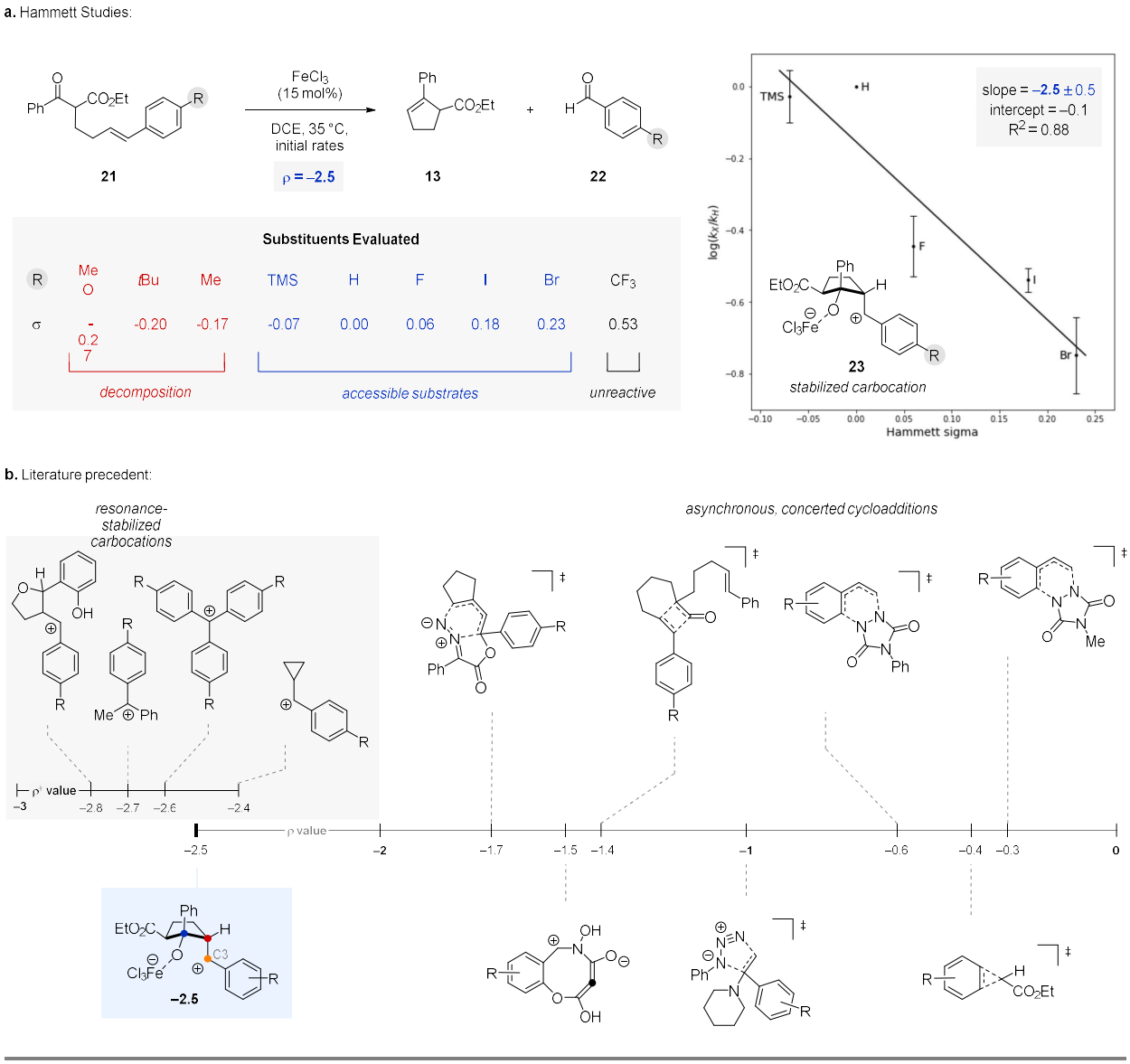

Figure 6. Hammett studies. (a) Initial rate data were gathered for substrates **21** differing in their para-substitution with 7 aliquots per replicate and 3–5 replicates per substrate. Electron-rich substrates gave decomposition, while electron-poor substrates were unreactive. (b) Relevant literature precedent of Hammett ρ and ρ^+ values. The observed slope is consistent with the generation of a stabilized carbocation (left), but not consistent with a concerted cycloaddition (right). (For references, see Supplementary Section 9).

Having established that both substrate classes proceed via the same stepwise mechanism, we conducted the proposed Hammett study. Analysis of the initial rates for a variety of different styrenes (Fig. 6) yielded a good correlation with the Hammett σ parameter ($\rho = -2.5 \pm 0.5$; $R^2 = 0.88$). The considerable rate acceleration afforded by electron-donating substituents is consistent with the generation of substantial positive charge at C3. Interestingly, we only observed a modest correlation with the Hammett σ^+ parameter. This decreased correlation could indicate that the cation is stabilized more by field effects, via the proximity between the positive charge at C3 and the negative charge at O1, and less by resonance effects from the neighboring aromatic ring.

However, the incompatibility of the reaction with strongly electron-donating substituents precludes a more detailed interpretation. Overall, the rate of carbonyl–olefin metathesis is greatly increased by electron-donating substituents, to an extent that is much larger than would be expected for a concerted cycloaddition (Fig 5b), but is consistent with a stepwise mechanism.

This body of experimental evidence consisting of $^{12}C/^{13}C$ KIE, Hammett, and β-SDKIE studies strongly supports the existence of a betaine intermediate and a stepwise pathway for iron(III)-catalyzed carbonyl–olefin metathesis. However, it is troubling that DFT calculations of nearly coupled-cluster quality predict a concerted mechanism instead. We hypothesize that this error is due to deficiencies in the treatment of solvation. While implicit solvent models perform well for neutral species (best-case root-mean-squared deviations of ~1 kcal/mol), such models perform much worse for ionic solutes (~6 kcal/mol) (*45*). As a result, implicit solvation is expected to be accurate for the relatively unpolarized ground state, but inaccurate for the charge-separated betaine. Hence, the cancellation of solvation errors is likely to be poor. This effect leads to the erroneous estimate that the betaine and the concerted transition state are as similar in energy in solution as they are in the gas phase (Fig. 7a and 7b), and thus the prediction of an incorrect mechanism.

This systematic error arises because implicit solvation models represent the solvent as a continuous field and are therefore unable to account for specific solute–solvent interactions (*30*). While the natural remedy is to model the solvent explicitly (*46–50*), this introduces many new degrees of freedom that require extensive sampling. Here, we immersed our model system in a sphere of 100 molecules of 1,2-dichloroethane (*51*) and chose to sample from the resulting ensemble by using *ab initio* molecular dynamics (AIMD) (*52–55*). To run the required simulations, we employed *presto* (*56*), an open-source Python program that enables the setup, running, and analysis of AIMD trajectories. Following equilibration, 130 replicates were constrained to various C1–C2 and C3–O1 bond distances and allowed to evolve for 20 ps each, for a total of 2.6 ns of simulation time. We then derived a two-dimensional free energy surface by using the weighted histogram analysis method (WHAM) (*57,58*).

In contrast to the predictions made in the gas phase or implicit solvent, these explicitly solvated calculations predict that the betaine exists as a stable intermediate (Fig. 7c). While these calculations are subject to the recognized limitations of current explicit-solvent methodology (including approximate energies, incomplete sampling (*59*), and possible non-equilibrium solvation effects) (*60*), we interpret the distinct betaine minimum as support for a classical stepwise mechanism (*61*). This result is consistent with our KIE and Hammett studies and shows that explicit solvation is needed to accurately describe iron(III)-catalyzed carbonyl–olefin metathesis.

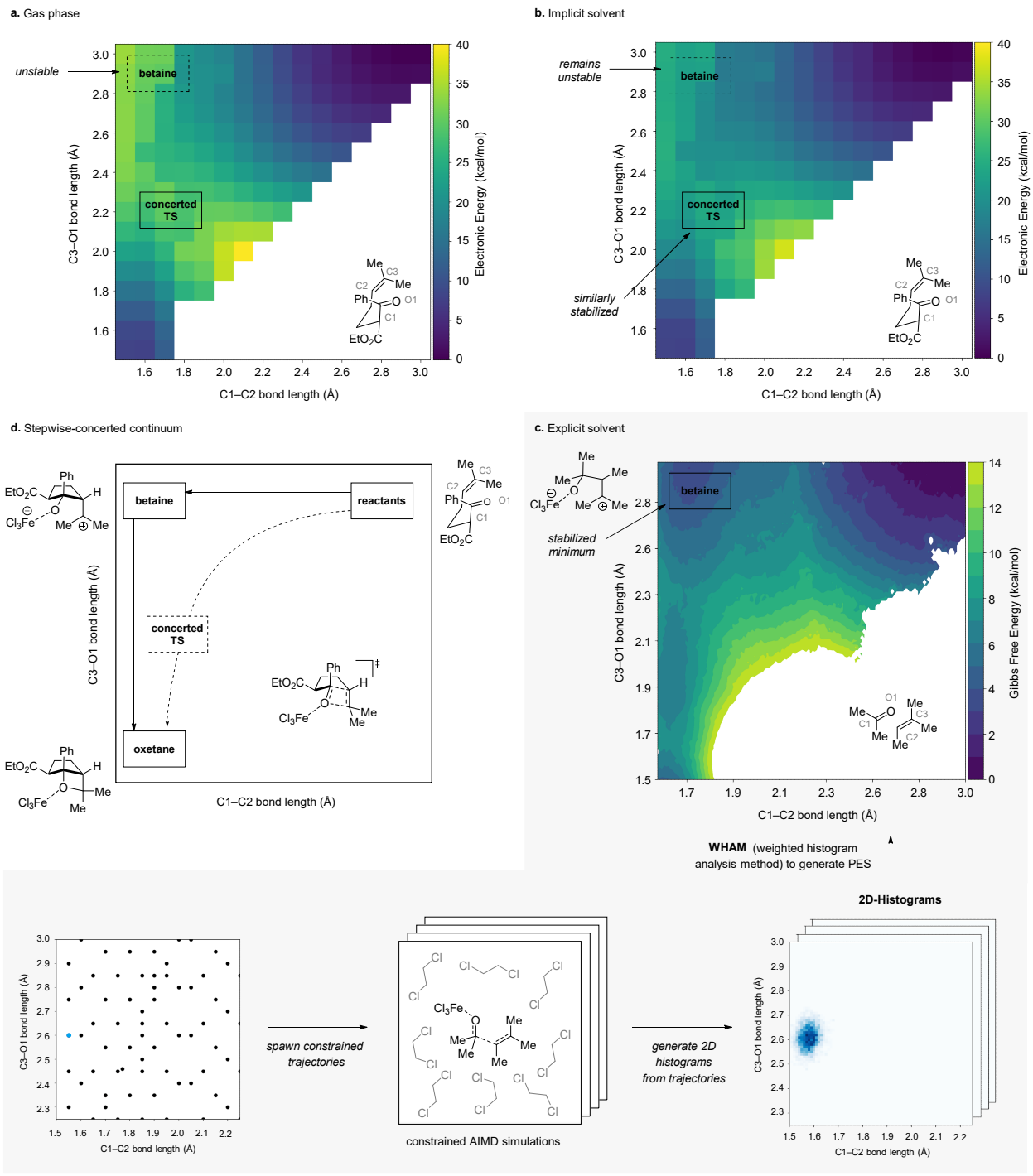

Figure 7. Solvation method affects the predicted mechanism. In both (a) the gas phase and (b) implicit solvent, the betaine is unstable and a concerted mechanism is predicted (B3LYP-D3(BJ)/jul-cc-pVDZ). In (c) explicit solvent, the betaine is stabilized (upper left-hand corner) and a stepwise mechanism is predicted (AIMD with B3LYP-D3(BJ)/MIDI!-LANL2DZ(Fe,Cl) for solutes and GFN0-xtb for solvent, reference *62*). The workflow used to generate a free energy surface from constrained AIMD simulations is illustrated below. (d) An idealized More O'Ferrall–Jencks plot.

Both the failure of implicit solvation to predict the correct stepwise mechanism and the influence of this error on the predicted KIEs can be understood by using Marcus theory (*63*). In general, the minimum energy path for cycloaddition can be regarded as the intersection of potentials for the reactants, betaine, and oxetane. In implicit solvent, the betaine curve is too high, causing the minimum energy path to involve only the reactants and oxetane (Fig. 8a). The resulting concerted transition state is positioned centrally between these species, involves a significant degree of bond cleavage and formation, and thus generates relatively large predicted KIEs for the concerted mechanism.

In explicit solvent, the betaine curve is much lower, causing it to intersect the minimum energy path as an intermediate with two flanking transition states. In Figure 8b, the first transition state (betaine formation, **16**) is depicted as rate-limiting, as is the case for prenyl substrate **10**. This transition state is late with respect to the reactants and the betaine, and is thus betaine-like. Alternatively, the second transition state (betaine collapse, **19**) could be rate-limiting, as it is for the styrenyl substrate **20**. This transition state is positioned early with respect to the betaine and oxetane, and is thus also betaine-like. In both structures, the bonds are nearly completely formed or broken, and thus relatively small KIEs are predicted for the stepwise mechanism.

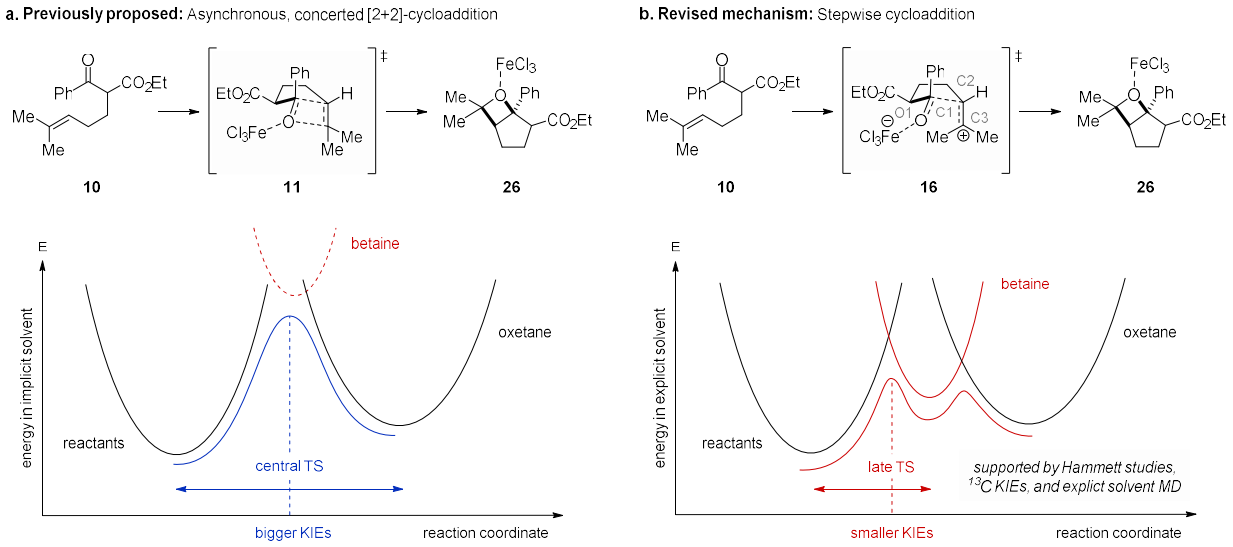

Figure 8. Marcus analysis. (a) In implicit solvent, the betaine curve is too high in energy to contribute to the minimum energy path and a concerted mechanism is predicted. The corresponding transition state is central between the reactants and oxetane and thus large KIEs are erroneously predicted. (b) In explicit solvent, the betaine curve is stabilized and intersects the reactant and oxetane potentials, resulting in the prediction of a stepwise mechanism. In the case depicted, betaine formation is rate-determining, the corresponding transition state is late and betaine-like, and small KIEs are correctly predicted.

a. Solvation Models in the Study of Organic Reaction Mechanisms

Implicit Solvation | **Explicit Solvation**

1981

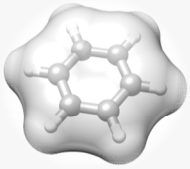

solvent is represented as continuous medium (PCM, COSMO, SMx models)

Diels-Alder Reaction (**1991**)

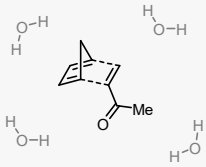

explicit solvation explains hydrophobic acceleration

Electrophilic Aromatic Substitution (S_EAr, **2016**)

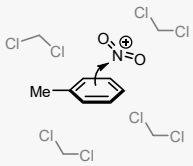

nitration is barrierless; regioselectivity is controlled by solvent reorganization

Glycosylation (**2021**)

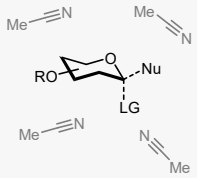

position along S_N1-S_N2 continuum is solvent dependent

b. Inadequacy of Continuum Solvation for the Prediction of Catalytic Carbonyl-Olefin Metathesis Reactions: Qualitative Change in Mechanism

gas phase | **implicit solvation** | **explicit solvation**

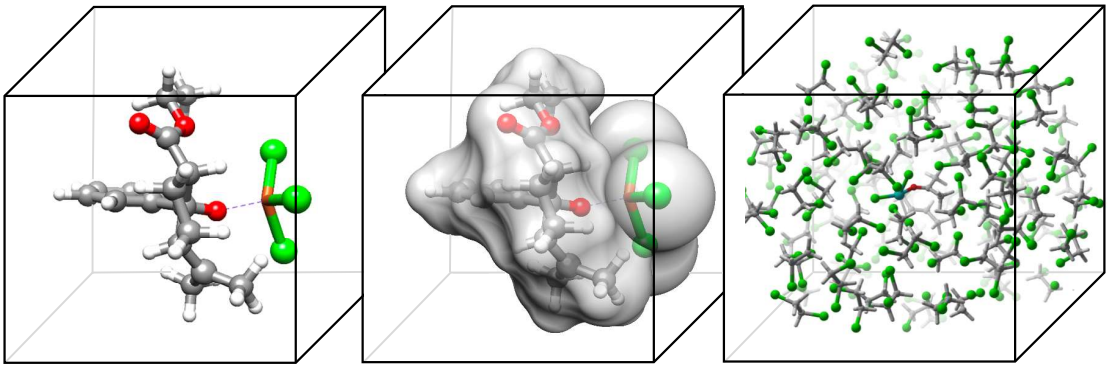

conventional transition state search | conventional transition state search | constrained trajectories and weighted-histogram analysis (WHAM)

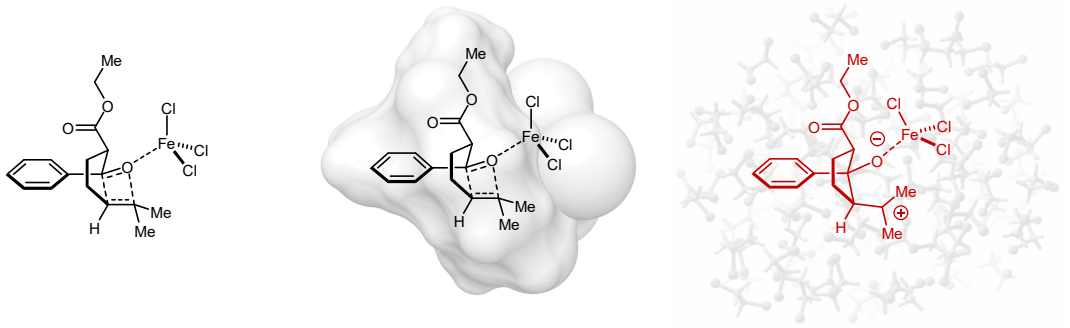

concerted mechanism | *concerted mechanism* | *stepwise mechanism*

c. Impact of Explicit Solvent on the Prediction of Polar Reaction Mechanisms

nonpolar | **polarized** | **charged**

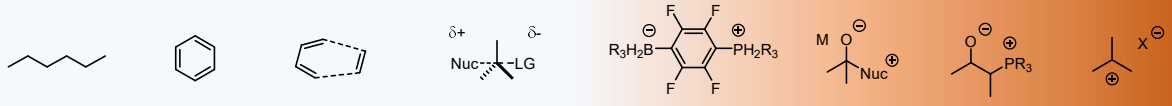

hydrocarbons | aromatics | Diels-Alder transition states | nucleophilic substitution (S_N2) | Frustrated Lewis Pairs (FLPs) | tetrahedral intermediate | Wittig olefination intermediate | ion pairs

high accuracy in gas phase and implicit solvent | ***low accuracy in gas phase and implicit solvent***

Figure 9. Solvation Models in Mechanistic Analysis. (a) Implicit solvation has been widely used for computational expediency in many systems. However, explicit solvent is needed when there are strong or specific solute–solvent interactions. (b) In carbonyl–olefin metathesis, a concerted mechanism is erroneously predicted in the gas phase or implicit solvent. The stepwise mechanism is correctly predicted in explicit solvent. (c) Explicit solvation becomes increasingly important as the structures under study become more polarized.

As the foregoing Marcus analysis shows, the balance between predicting stepwise and concerted mechanisms hinges on the stability of the betaine relative to the intersection of the reactant and product curves. These points are close enough in energy to be within the uncertainty of implicit solvent models, and the results are catastrophic. Despite this, the predicted mechanism remained plausible, and the comprehensive experimental studies detailed here were needed to detect the issue.

Fortunately, the correct prediction does emerge from explicit solvent calculations. This approach has a rich history (Fig. 10a). In the 1990s, the Jorgensen group pioneered the development of explicit solvation methods (*20*) and have applied them to the study of many systems, including "on-water" Diels–Alder reactions (*64,65*). More recently, the Singleton group has convincingly demonstrated the importance of explicit solvent in modeling selectivity in several systems (*46, 60, 62*), including regioselectivity in the nitration of toluene (*46*). Similarly, the Liu group has shown that explicit solvation models can help rationalize the mechanistic course of glycosylation reactions (*48*).

Despite these successes, explicit solvation is rarely used for mechanistic studies because it is commonly assumed that implicit solvation is "good enough" for routine applications. This must change. Historically, the accuracy of predictions has been primarily constrained by the underestimation of electron correlation and basis set incompleteness. Now, the advent of sophisticated density functionals, balanced basis sets, and greater computational power have greatly reduced such errors (*22*, *29*, *32*). In this case, the model chemistry is nearly of coupled-cluster/complete-basis-set quality and, by this conventional metric, could have been declared "chemically accurate" (*32*).

Nonetheless, the predicted mechanism was incorrect. The failure of computational best practices to recapitulate the stepwise mechanism here reveals a hidden failure mode of conventional protocols that may be rather common: when charge separation develops along the reaction path, poor error cancellation between the ground and transition states can lead to qualitatively incorrect predictions (Fig. 10c). The fact that explicit solvation is not typically used, even when it should be, reflects the substantial complexity and cost of the required calculations. Thus, our study is a call to action: more realistic and practical methods for the treatment of solvation are keenly needed, particularly for the study of reactions involving polarized intermediates (*47*, *60*, *62*, *66*, *67*).

References and Notes

1. A. C. Jackson, B. E. Goldman, B. B. Snider, Intramolecular and intermolecular Lewis acid catalyzed ene reactions using ketones as enophiles. *J. Org. Chem.* **49**, 3988–3994 (1984).

2. H. -P. van Schaik, R. -J. Vijn, F. Bickelhaupt, Acid-catalyzed olefination of benzaldehyde. *Angew. Chem. Int. Ed.* **33**, 1611–1612 (1994).
3. A. Soicke, N. Slavov, J. -M. Neudörf, H. -G. Schmalz, Metal-free intramolecular carbonyl–olefn metathesis of *ortho*-prenylaryl ketones. *Synlett* **17**, 2487–2490 (2011).
4. A. K. Griffith, C. M. Vanos, T. H. Lambert, Organocatalytic carbonyl−olefin metathesis. *J. Am. Chem. Soc.* **134**, 18581–18584 (2012).
5. V. R. Naidu, J. Bah, J. Franzén, Direct organocatalytic oxo-metathesis, a *trans*-selective carbocation-catalyzed olefination of aldehydes. *Eur. J. Org. Chem.* **2015**, 1834–1839 (2015).
6. J. R. Ludwig, P. M. Zimmerman, J. B. Gianino, C. S. Schindler, Iron(iii)-catalysed carbonyl–olefin metathesis. *Nature* **533**, 374–379 (2016).
7. L. Ma, et al. $FeCl_3$-catalysed ring-closing carbonyl–olefin metathesis. *Angew. Chem. Int. Ed.* **55**, 10410–10413 (2016).
8. J. R. Ludwig, et al. Mechanistic investigations of the iron(iii)-catalysed carbonyl–olefin metathesis reaction. *J. Am. Chem. Soc.* **139**, 10832–10842 (2017).
9. L. Catti, K. Tiefenbacher, Bronsted acid-catalyzed carbonyl–olefin metathesis inside a self-assembled supramolecular host. *Angew. Chem., Int. Ed.* **57**, 14589−14592 (2018).
10. U. P. N. Tran, G. Oss, D. P. Pace, J. Ho, T. V. Nguyen, Tropylium-promoted carbonyl–olefin metathesis reactions. *Chem. Sci.* **9**, 5145–5151 (2018).
11. U. P .N. Tran, et al. Carbonyl–olefin metathesis catalysed by molecular iodine. *ACS Catal.* **9**, 912–919 (2019).
12. C. S. Hanson, M. C. Psaltakis, J. J. Cortes, J. J. Devery, Catalyst behavior in metal-catalyzed carbonyl–olefin metathesis. *J. Am. Chem. Soc.* **141**, 11870–11880 (2019).
13. A. Djurovic, et al. Synthesis of medium-sized carbocycles by gallium-catalysed tandem carbonyl–olefin metathesis/transfer hydrogenation. *Org. Lett.* **21**, 8132–8137 (2019).
14. R. Wang, et al. $AuCl_3$-catalyzed ring-closing carbonyl–olefin metathesis. *Chem. Eur. J.* **26**, 1941–1946 (2020).
15. T. A. To, C. Pei, R. Koenigs, T. V. Nguyen, Hydrogen bonding networks enable Brønsted acid-catalyzed carbonyl–olefin metathesis. *Angew. Chem., Int. Ed.* **61**, e202117366 (2022).
16. M. R. Becker, J. P. Reid, K. Rykaczewski, C. S. Schindler, Models for understanding divergent reactivity in Lewis acid-catalyzed transformations of carbonyls and olefins. *ACS Catal.* **10**, 4387–4397 (2020).
17. A. J. Davis, R. B. Watson, D. J. Nasrallah, J. L. Gomez-Lopez, C. S. Schindler, Superelectrophilic aluminium(iii)–ion pairs promote a distinct reaction path for carbonyl–olefin ring-closing metathesis. *Nat. Catal.* **3**, 787–796 (2020).
18. H. Albright, et al. Carbonyl–olefin metathesis. *Chem. Rev.* **121**, 9359–9406 (2021).
19. J. Gao, Hybrid quantum and molecular mechanical simulations: An alternative avenue to solvent effects in organic chemistry. *Acc. Chem. Res.* **29**, 298–305 (1996).

20. W. L. Jorgensen, Free energy calculations: a breakthrough for modeling organic chemistry in solution. *Acc. Chem. Res.* **22**, 184–189 (1989).

21. G. -J. Cheng, X. Zhang, L. W. Chung, L. Xu, Y. -D. Wu, Computational organic chemistry: Bridging theory and experiment in establishing the mechanisms of chemical reactions. *J. Am. Chem. Soc.* **137**, 1706–1725 (2015).

22. A. D. Becke, Perspective: Fifty years of density-functional theory in chemical physics. *J. Chem. Phys.* **140**, 18A301 (2014).

23. A. J. DelMonte, J. Haller, K. N. Houk, K. B. Sharpless, D. A. Singleton, T. Strassner, A. A. Thomas, Experimental and theoretical kinetic isotope effects for asymmetric dihydroxylation. Evidence supporting a rate-limiting "(3 + 2)" cycloaddition. *J. Am. Chem. Soc.* **119**, 9907–9908 (1997).

24. E. E. Kwan, Y. Zeng, H. A. Besser, E. N. Jacobsen, Concerted nucleophilic aromatic substitutions. *Nat. Chem.* **10**, 917–923 (2018).

25. H. J. A. Dale, A. G. Leach, G. C. Lloyd-Jones, Heavy-atom kinetic isotope effects: Primary interest or zero point? *J. Am. Chem. Soc.* **143**, 21079–21099 (2021).

26. G. Adames, C. Bibby, R. Grigg, Rhodium(I) catalysed rearrangements of vinyl epoxides and oxetans. *J. Chem. Soc., Chem. Commun.,* 491–492 (1972).

27. H. A. J. Carless, H. S. Trivedi, New ring expansion reaction of 2-t-butyloxetanes. *J. Chem. Soc., Chem. Commun.,* 382–383 (1979).

28. B. Mennucci, Polarizable continuum model. *Wiley Interdiscip. Rev. Comput. Mol. Sci.* **2**, 386–404 (2012).

29. R. A. Mata, M. A. Suhm, Benchmarking quantum chemical methods: Are we heading in the right direction? *Angew. Chem. Int. Ed.* **56**, 11011–11018 (2017).

30. H. Ryu, J. Park, H. K. Kim, J. Y. Park, S. -T. Kim, M. Baik, Pitfalls in computational modeling of chemical reactions and how to avoid them. *Organometallics* **37**, 3228–3239 (2018).

31. M. Bursch, J. -M. Mewes, A. Hansen, S. Grimme, Best-practice DFT protocols for basic molecular computational chemistry. *Angew. Chem. Int. Ed.*, **61**, e202205735 (2022).

32. Y. Guo, et al. Communication: An improved linear scaling perturbative triples correction for the domain based local pair-natural orbital based singles and doubles coupled cluster method [DLPNO-CCSD(T)]. *J. Chem. Phys.* **148**, 011101 (2018).

33. T. J. Lee, P. R. Taylor, A diagnostic for determining the quality of single-reference electron correlation methods. *Int. J. Quantum Chem.* **36**, 199–207 (1989).

34. B. Li, Y. Li, Y. Dang, K. N. Houk, Post-transition state bifurcation in iron-catalyzed arene aminations. *ACS Catal*. **11**, 6816–6824 (2021).

35. D. A. Singleton, A. A. Thomas, High-precision simultaneous determination of multiple small kinetic isotope effects at natural abundance. *J. Am. Chem. Soc.* **117**, 9357–9358 (1995).

36. E. E. Kwan, Y. Park, H. A. Besser, T. L. Anderson, E. N. Jacobsen, Sensitive and accurate ^{13}C kinetic isotope effect measurements enabled by polarization transfer. *J. Am. Chem. Soc.* **139**, 43–46 (2017).

37. J. S. Hirschi, T. Takeya, C. Hang, D. A. Singleton, Transition-state geometry measurements from ^{13}C isotope effects. The experimental transition state for the epoxidation of alkenes with oxaziridines. *J. Am. Chem. Soc.* **131**, 2397–2403 (2009).

38. V. L. Schramm, Enzymatic transition states, transition-state analogs, dynamics, thermodynamics, and lifetimes. *Annu. Rev. Biochem.* **80**, 703–732 (2011).

39. M. -H. Zhuo, D. J. Wilbur, E. E. Kwan, C. S. Bennet, Matching glycosyl donor reactivity to sulfonate leaving group ability permits S_N2 glycosylations. *J. Am. Chem. Soc.* **141**, 16743–16754 (2019).

40. A. J. Kresge, N. N. Lichtin, K. N. Rao, R. E. Weston Jr., The primary carbon isotope effect on the ionization of triphenylmethyl chloride. Experimental determination, theoretical justification, and implications for carbon isotope effects on nucleophilic substitution at saturated carbon.[1-3] *J. Am. Chem. Soc.* **87**, 437–445 (1965).

41. V. J. Shiner Jr., Deuterium isotope effects and hyperconjugation. *Tetrahedron* **5**, 243–252 (1959).

42. L. M. Stephenson, M. Orfanopoulos, Changes in ene reaction mechanisms with Lewis acid catalysis. *J. Org. Chem.* **46**, 2200–2201 (1981).

43. M. P. Meyer, A. J . DelMonte, D. A. Singleton, Reinvestigation of the isotope effects for the Claisen and aromatic Claisen rearrangements: The nature of the Claisen transition states. *J. Am. Chem. Soc.* **121**, 10865–10874 (1999).

44. D. A. Singleton, C. Hang, ^{13}C and ^{2}H kinetic isotope effects and the mechanism of Lewis acid-catalyzed ene reactions of formaldehyde. *J. Org. Chem.* **65**, 895–899 (2000).

45. A. V. Marenich, C. J. Cramer, D. G. Truhlar, Universal solvation model based on solute electron density and on a continuum model of the solvent defined by the bulk dielectric constant and atomic surface tensions. *J. Phys. Chem. B* **113**, 6378–6396 (2009).

46. Y. Nieves-Quinones, D. A. Singleton, Dynamics and regiochemistry of nitration of toluene. *J. Am. Chem. Soc.* **138**, 15167–15176 (2016).

47. A. Eilmes, P. Kubisiak, M. Brela, Explicit solvent modelling of IR and UV–Vis spectra of 1-ethyl-3-methylimidazolium bis(trifluoromethylsulfonyl)imide ionic liquid. *J. Phys. Chem. B* **120**, 11026–11034 (2016).

48. Y. Fu, L. Bernasconi, P. Liu, Ab Initio molecular dynamics simulations of the S_N1/S_N2 mechanistic continuum in glycosylation reactions. *J. Am. Chem. Soc.* **143**, 1577–1589 (2021).

49. R. Van Lommel, J. Bock, C. G. Daniliuc, U. Hennecke, F. De Proft, A dynamic picture of the halolactonization reaction through a combination of *ab initio* metadynamics and experimental investigations. *Chem. Sci.* **12**, 7746–7757 (2021).

50. L. Martínez, R. Andrade, E. G. Bergin, J. M. Martínez, PACKMOL: A package for building initial configurations for molecular dynamics simulations. *J. Comput. Chem.* **30**, 2157–2164 (2009).

51. L. W. Chung, et al. The ONIOM method and its applications. *Chem. Rev.* **115**, 5678–5796 (2015).

52. C. Bannwarth, et al. Extended tight-binding quantum chemistry methods. *Wiley Interdiscip. Rev. Comput. Mol. Sci.* **11**, e1493 (2021).

53. P. Vidossich, A. Lledós, G. Ujaque, First-principles molecular dynamics studies of organometallic complexes and homogeneous catalytic processes. *Acc. Chem. Res.* **49**, 1271–1278 (2016).

54. R. M. Peltzer, J. Gauss, O. Eisenstein, M. Cascella, The Grignard reaction – Unraveling a chemical puzzle. *J. Am. Chem. Soc.* **142**, 2984–2994 (2020).

55. T. D. Kühne, Second generation Car–Parrinello molecular dynamics. *Wiley Interdiscip. Rev. Comput. Mol. Sci.* **4**, 391–406 (2014).

56. C. C. Wagen, *presto*. github.com/corinwagen/presto, (2021).

57. A. Grossfeld, WHAM: The weighted histogram analysis method, version 2.0.11, http://membrane.urmc.rochester.edu/wordpress/?page_id=126.

58. S. Kumar, J. M. Rosenberg, D. Bouzida, R. H. Swendsen, P. A. Kollman, The weighted histogram analysis method for free-energy calculations on biomolecules. I. The method. *J. Comput. Chem*., **13**, 1011–1021 (1992).

59. E. Crabb, et al. Importance of equilibration method and sampling for *ab Initio* molecular dynamics simulations of solvent–lithium-salt systems in lithium-oxygen batteries. *J. Chem. Theory Comput.* **16**, 7255–7266 (2020).

60. Z. Chen, Y. Nieves-Quinones, J. R. Waas, D. A. Singleton, Isotope effects, dynamic matching, and solvent dynamics in a Wittig reaction. Betaines as bypassed intermediates. *J. Am. Chem. Soc.* **136**, 13122–13125 (2014).

61. R. E. Plata, D. A. Singleton, A case study of the mechanism of alcohol-mediated Morita Baylis–Hillman reactions. The importance of experimental observations. *J. Am. Chem. Soc.* **137**, 3811–3826 (2015).

62. V. A. Roytman, D. A. Singleton, Solvation dynamics and the nature of reaction barriers and ion-pair intermediates in carbocation reactions. *J. Am. Chem. Soc.* **142**, 12865–12877 (2020).

63. R. A. Marcus, N. Sutin, Electron transfers in chemistry and biology. *Biochim. Biophys. Acta* **811**, 265–322 (1985).

64. J. F. Blake, W. L. Jorgensen, Solvent effects on a Diels-Alder reaction from computer simulations. *J. Am. Chem. Soc.* **113**, 7430–7432 (1991).

65. J. F. Blake, D. Lim, W. L. Jorgensen, Enhanced hydrogen bonding of water to Diels-Alder transition states. Ab initio evidence. *J. Org. Chem.* **59**, 803–805 (1994).

66. Y. I. Yang, Q. Shao, J. Zhang, L. Yang, Y. Q. Gao, Enhanced sampling in molecular dynamics. *J. Chem. Phys.* **151**, 070902 (2016).

67. M. Souaille, B. Roux, Extension to the weighted histogram analysis method: combining umbrella sampling with free energy calculations. *Comput. Phys. Commun.* **135**, 40–57 (2001).

Acknowledgments: We thank the NIH/National Institute of General Medical Sciences (R01 GM118644), the Alfred P. Sloan Foundation, the David and Lucile Packard Foundation and the Camille and Henry Dreyfus Foundation for financial support. H.L.V. thanks the

Rackham Graduate School at the University of Michigan for a predoctoral fellowship. C.C.W thanks the NSF for financial support through the Graduate Research Fellowship Program (DGE1745303). We thank Dr. Eugenio Alvarado for helpful guidance with setting up NMR experiments. We thank Katherine Forbes, Marcus Sak, Hayden Sharma, and Daniel Singleton for helpful discussions. Further acknowledgements can be found in Supplemental Section 1.

Author contributions:

Conceptualization: HLV, EEK, CSS

Synthesis of substrates and intermediates: HLV

Key substrate purifications: SEM

Reaction optimization and experimental studies: HLV

Data analysis: HLV, EEK

Computational studies: CCW, JBT, EEK

Supervision: EEK, CSS

Writing: HLV, CCW, EEK, CSS

Competing interests: Authors declare that they have no competing interests.